China Geology 4 (2018) 493−504

China Geology

Journal homepage: http://chinageology.cgs.cn

Distribution of gas hydrate reservoir in the first production test region of the Shenhu area, South China Sea

Ru-wei Zhang*, Jing-an Lu, Pen-fei Wen, Zeng-gui Kuang, Bao-jin Zhang, Hua Xue, Yun-xia Xu, Xi Chen

Guangzhou Marine Geological Survey, China Geological Survey, Guangzhou 510075, *China*

ARTICLE INFO

Article history:
Received 15 August 2018
Received in revised form 30 October 2018
Accepted 2 November 2018
Available online 3 December 2018

Keywords:
Shenhu area
Gas hydrate
Production test
Reservoir distribution

ABSTRACT

In May and July of 2017, China Geological Survey (CGS), and Guangzhou Marine Geological Survey (GMGS) carried out a production test of gas hydrate in the Shenhu area of the South China Sea and acquired a breakthrough of two months continuous gas production and nearly 3.1×10^5 m^3 of production. The gas hydrate reservoir in the Shenhu area of China, is mainly composed of fine-grained clay silt with low permeability, and very difficult for exploitation, which is very different from those discovered in the USA, and Canada (both are conglomerate), Japan (generally coarse sand) and India (fracture-filled gas hydrate). Based on 3D seismic data preserved-amplitude processing and fine imaging, combined with logging-while-drilling (LWD) and core analysis data, this paper discusses the identification and reservoir characterization of gas hydrate orebodies in the Shenhu production test area. We also describe the distribution characteristics of the gas hydrate deposits and provided reliable data support for the optimization of the production well location. Through BSR feature recognition, seismic attribute analysis, model based seismic inversion and gas hydrate reservoir characterization, this paper describes two relatively independent gas hydrate orebodies in the Shenhu area, which are distributed in the north-south strip and tend to be thicker in the middle and thinner at the edge. The effective thickness of one orebody is bigger but the distribution area is relatively small. The model calculation results show that the distribution area of the gas hydrate orebody controlled by W18/W19 is about 11.24 km^2, with an average thickness of 19 m and a maximum thickness of 39 m, and the distribution area of the gas hydrate orebody controlled by W11/W17 is about 6.42 km^2, with an average thickness of 26 m and a maximum thickness of 90 m.

1. Introduction

Natural gas hydrate (NGH) is a clathrate compound composed of natural gas and water under low-temperature and high-pressure conditions (Sloan ED, 1990), and referred to as “Fire Ice”, present a high density, wide distribution, huge size and concealed shallows. The amount of NGH resources is equivalent to two times the world's total reserves of coal, oil and natural gas. (Jin QH et al., 2006; Zhang HT et al., 2007). NGH is widespread in the high-latitude permafrost regions of China and the shallow sediments of the South China Sea (SCS) (Li W et al., 2013). The investigation of NGH in China started in 1999 in the Xisha trough of SCS. In March and June 2007, NGH samples were collected by the Guangzhou Marine Geological Survey (GMGS) in the Shenhu area of SCS. Subsequently, eleven spots for NGH mining were delineated with a predicted potential of 1.94×10^{11} m^3 (Zhang HT et al., 2007). In the second half of 2013, GMGS drilled 13 drilling sites in the eastern Pearl River mouth basin of the northern slope, SCS. A large number of NGH samples of various types (massive, tumorous, stratiform, veined and dispersed) have been obtained again (Zhang GX et al., 2014; Sha ZB et al., 2015). In 2015, GMGS drilled in the Shenhu eastern area again. Two large-scale NGH orebodies were found. And a small amount of type II NGH was found (Zhang W et al., 2018; Guo YQ et al., 2017; Zhang W et al., 2017). In May and July of 2017, GMGS carried out a production test of NGH in the Shenhu area of SCS and acquired a breakthrough of two months continuous gas production and nearly 3.1×10^5 m^3 of production (Li JF et al., 2018; Ye JL et al., 2018).

The seismic technique is the main method in use for detecting NGH. A bottom simulating reflector (BSR) on the seismic imaging section is an obvious sign of the existence of NGH and can be used for direct identification of NGH (Ma

* Corresponding author: *E-mail address*: cgszrw@163.com (Ru-wei Zhang).

doi:10.31035/cg2018049
2096-5192/© 2018 China Geology Editorial Office.

ZT et al., 2000; Auguy C et al., 2017). BSR can be identified on seismic profiles, mainly based on the following features: (1) simulated seafloor geomorphology; (2) a polarity contrary to the seafloor reflection; (3) generally crosscut with existing sedimentary strata (Dewangan P et al., 2014). BSR is also considered to be the base of the gas hydrate stability zone (GHSZ), because the isotherms are approximately parallel to the seafloor, so the bottom of the stable zone is usually parallel to the seafloor (Song HB et al., 2003; Wang LF et al., 2017; Horozal S et al., 2017). The appearance of BSR indicates that there is a difference in impedance. The high impedance above BSR is explained by NGH, while the low impedance below BSR is generally explained by free gas (Ma ZT et al., 2000; Yuan T et al., 1998).

With the amount of NGH increases, the velocities of P-wave and S-wave increase gradually (Sign S et al., 1993; Song HB et al., 2001). Therefore, NGH can be identified and estimated by its seismic velocity. Most of the seismic prediction methods of NGH originate from this basis (Carcione J and Tinivella U, 2000; Gei D and Carcione J, 2003; Chand S et al., 2010). Ecker C et al. (2000) predicted and estimated the distribution and saturation of NGH in the Black Ridge of North America by stack velocity analysis, and the saturation is about 12%. Based on this method, Liang J et al. (2013) also studied the distribution and variation of the acoustic velocity and the seismic velocity of NGH sediments in the Shenhu area. Xu HN et al. (2014) used pseudo-well constrained inversion of post-stack data. The results show that there are still high-velocity sediments beneath the NGH at SH7 station in the Shenhu area. Based on the joint data of 3D high-resolution seismic and ocean bottom seismographics (OBS), Zhang GX et al. (2014) determined the distribution of NGH sediments in the Shenhu area by using the S-wave and P-wave velocity obtained from travel-time inversion. Zhang RW et al. (2015) analyzed the distribution of NGH sediments in the Shenhu area by the P-S wave velocity ratios from the prestack three-parameter simultaneous inversion.

Through the analysis of some research results in the Shenhu area (Zhang W et al., 2017; Jin JP et al., 2017; Guo YQ et al., 2017; Su PB et al., 2017), the seismic characteristics of NGH are described in most literature, but the description of the hydrate reservoir is still in the qualitative stage, and the distribution of the reservoir boundary and thickness is not fine enough to meet the needs of selection for a production test well. In this paper, with the constraints of favorable reservoir characteristics (top and bottom depth, logging response etc.) for production tests, combined with core analysis data, and the fine distribution prediction of production tests NGH reservoir can be described in detail by the model-based impedance inversion (Russell B and Hampson D, 1991; Zhang RW et al., 2012), which provides a basis for determining the production test well location.

2. Characteristics of the gas hydrate

2.1. Geological background

The production test area is located in the middle of the continental slope of the southeastern Shenhu area, and northern SCS between Xisha Trough and Dongsha Islands (Su PB et al., 2014; Fu SY and Lu JA, 2010). The water depth is about 800 m to 1600 m, and the test area is about 320 km from Zhuhai city (Fig. 1a). Seamounts, hills, erosion ditches, downward slope ridges and submarine canyons are the main types of submarine topography (Fig. 1b). The topographic features are generally characterized by four valleys and three ridges (Su PB et al., 2014; Wang JL et al., 2015; Liang J et al., 2013; Li W et al., 2013). The valley bottom topography is flat, and part of the bottom topography has obvious fluctuation. The valley slope is steeper, and the slump is strong. The topography of the ridges is the most rugged and the slump is strong. The far end of the valley is flat. The overall gradient is relatively smooth, with an average of 4.5° and a maximum gradient of about 38°. The steepest place is located at the valley slope, and the slowest area is the bottom of the valley and the distal sedimentary area of the valley. The eastern slope is obviously steeper than the west side. The range of slope is less than 5° and is mainly distributed in the valley bottom and the flat area of the ridge. The range of slope greater than 5° is mainly distributed in the valley slope and the undulating area of ridge.

The Shenhu production test area is in the second depression of the Pearl River Mouth Basin. Since the late Miocene, the main structural activities are faulting, and faults in this area are generally developed. The faults are most developed in the Pliocene, and can be divided into three groups: NE, NW and NE trending, all of which are normal faults. Quaternary reflective interface faults have an obvious inheritance from Pliocene faults, but the NE and NE trending faults are more prominent. This indicates that the NE trending tectonic forces in the production test area have been weakening since the Pliocene, mainly showing the modern tectonic processes such as collapse and slip (Kuang ZG et al., 2011; Zeng XM et al., 2013; Lei XM et al., 2009). Some faults are still in activity and belong to active faults. These faults play a major channel role for fluid migration in the bottom source rocks. In the later stage, a large number of diapir structures were formed in the middle of the depression due to compression. The submarine diapir and oil source faults together become the main channels for fluid migration (Gong YH et al., 2009). Fig. 2 is the fracture, diapir structure and BSR reflection characteristics in the Shenhu production test area.

2.2. Characteristics of the production test deposit

According to the logging interpretation and the results from the core analysis of SHSC-4, the NGH reservoir is distributed between 201−236 mbsf, and there is associated free gas below. The reservoir lithology is clayey silt, whereas, the mean effective porosity is 35%, the mean hydrate saturation is 34%, and the mean permeability is 2.9 mD. The high content of clay minerals results in high bound water concentration of more than 65%, the mean median grain size

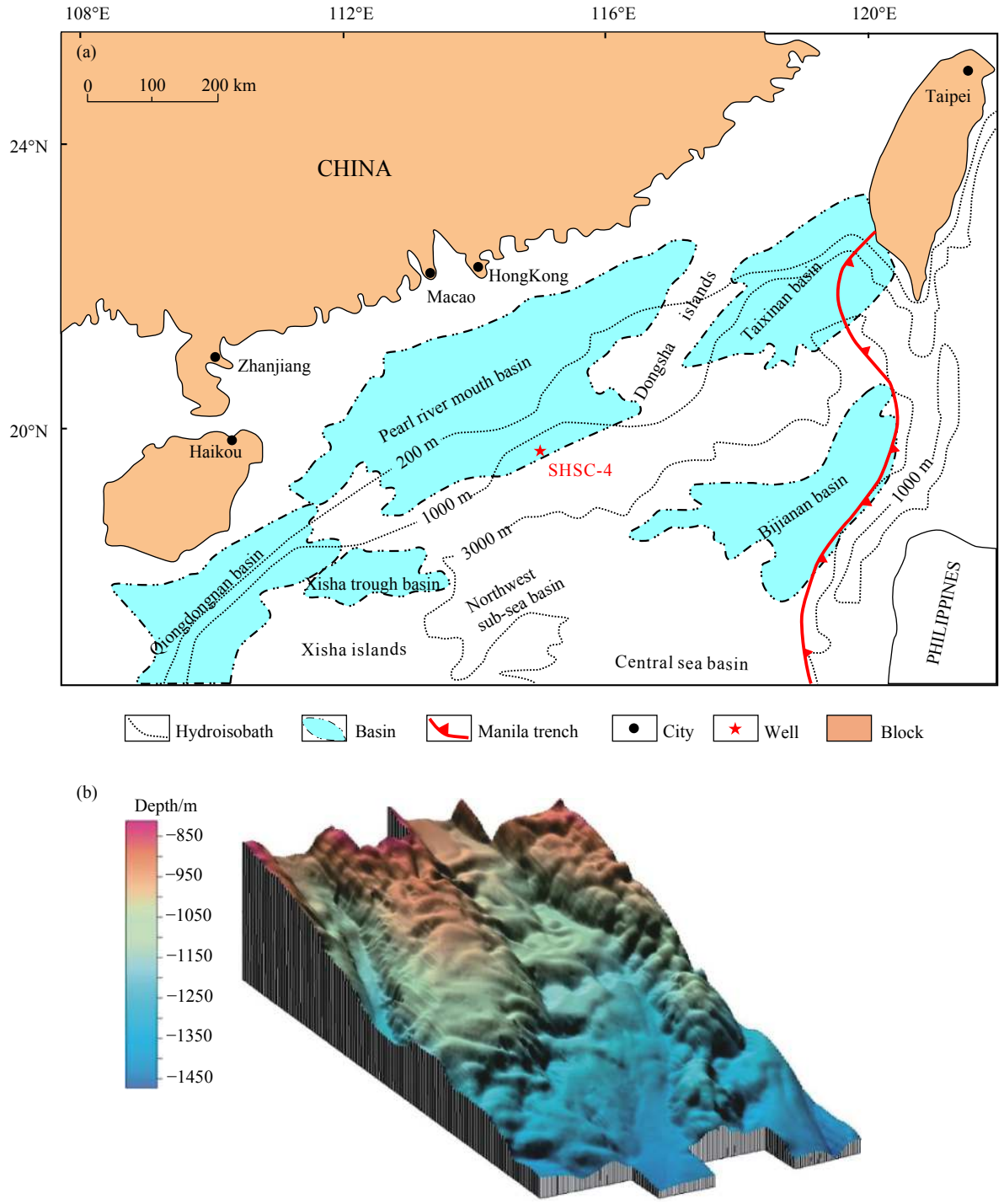

Fig. 1. Gas hydrate environments effect on survey areas, the production test location (a, modified from Li JF et al., 2018) and topography (b) in SCS.

of the sediments is about 12 μm. The minerals are mainly quartz-feldspathic (53%), carbonates (16%) and clay minerals (26%−30%), which are mainly montmorillonite and illite (Li JF et al., 2018).

3. Data and BSR

3.1. Seismic data

The acquisition of pseudo-3D seismic data from single source and single cable was completed by the "Fengdou Si" vessel of GMGS from April to June 2008, which lasted 59 days. 283 three-dimensional (3D) multi-channel seismic lines with 50 m spacing were completed, totaling 4171.1 km and covering an effective area of 159.75 km^2. The number of cables are 192, the spacing of cables is 12.5 m, the spacing of guns is 25 m, the minimum offset is 125 m, the sampling rate is 1 ms, the recording length is 5 s, and the original panel size is 12.5 m × 50 m. The original seismic data contains strong background noise interference, but the frequency band is wider. The frequency bandwidth analysis with −20 dB shows that the high frequency can reach 150 Hz and the main

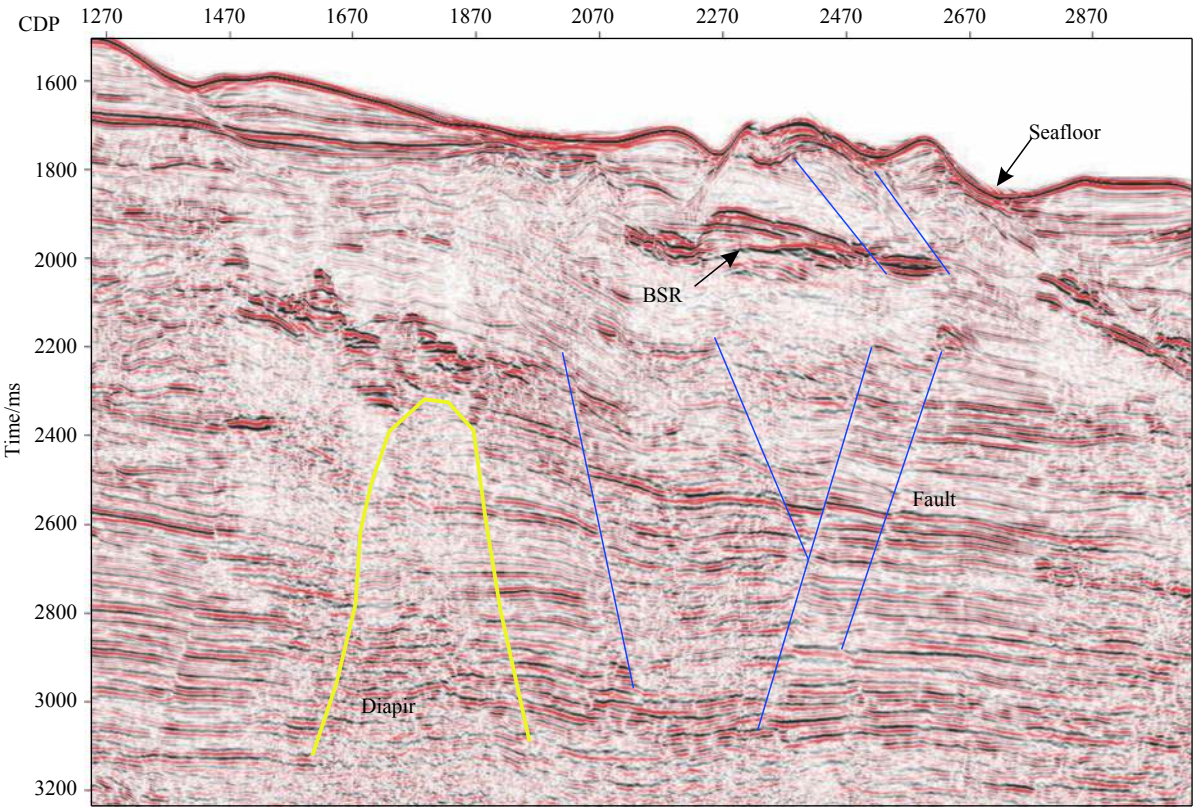

Fig. 2. Diapir structure and faults in the seismic profile.

frequency is about 70 Hz. Noise types mainly include: swell noise, large-value interference, linear interference and multiples.

Before the prediction of NGH reservoirs, pseudo-3D seismic data have been processed by background noise suppression, complex multiples attenuation, deconvolution, bin regularization, grid tomographic velocity modeling and prestack depth migration. Using 2–4 Hz low-cut filtering and abnormal amplitude attenuation (AAA) technology, the background noise can be suppressed better, and the effective reflection signal can be highlighted with amplitude preservation. Surface related multiple elimination (SRME), deconvolution, high precision Radon transform and frequency division attenuation diffraction multiples (Zhang RW et al., 2016) are combined to attenuate various complex multiples and improve the signal-to-noise ratio. Based on the grid tomography and prestack depth migration technology, high precision velocity model and seismic imaging effects are obtained.

3.2. Characteristics of BSR

BSR is a negative reflection coefficient, which reveals that the negative acoustic impedance reflectivity is generally due to the presence of a small amount of NGH in the sediments and the presence of low-velocity free gas zones underlying the sediments, or the presence of irregularly distributed high-velocity hydrate sediments, and the underlying strata are saturated sediments with background velocities. The velocity models represent two different NGH formations. The former model predicts the existence of free gas under BSR, which is generally called the “free gas model”, while the latter model predicts the characteristics of NGH enrichment near BSR, which can be called the “hydrate wedge model” (Katzman R et al., 1999; Song HB et al., 2003).

The NGH reservoir zone in the Shenhu area of SCS is characterized by strong BSR at the bottom, amplitude-enhanced reflector (gas accumulation area) below the BSR (Fig. 3). Faults develop at the bottom, which is favorable for gas migration and accumulation of gas hydrate stable regions. BSR is distributed around CDP # 2290−2730 and the BSR is about 250 m from the seafloor. The amplitude is relatively continuous and strong, but the distribution range is relatively small. Below the BSR, there are strong energy reflection amplitudes formed by free gas, and a fault and reflection blurred area (gas migration channel) in the lower part, indicating that NGH in this area is the typical “free gas model”.

Also, the occurrence of NGH and free gas in this area can be reflected by the AVA (amplitude varying with incident angle) characteristics of BSR (Ecker C et al., 1998; Zhang RW et al., 2011; Ehsan MI et al., 2016). Fig. 4 shows the seismic migration stack section, common imaging gathers and AVA characteristics of BSR. The characteristics of BSR on the seismic migration stack section are relatively clear and continuous and traceable, which is very similar to the topography of the seafloor, and also have obvious characteristics of cut cross with existing sedimentary strata (Fig. 4a). BSR shows the characteristics of medium strong

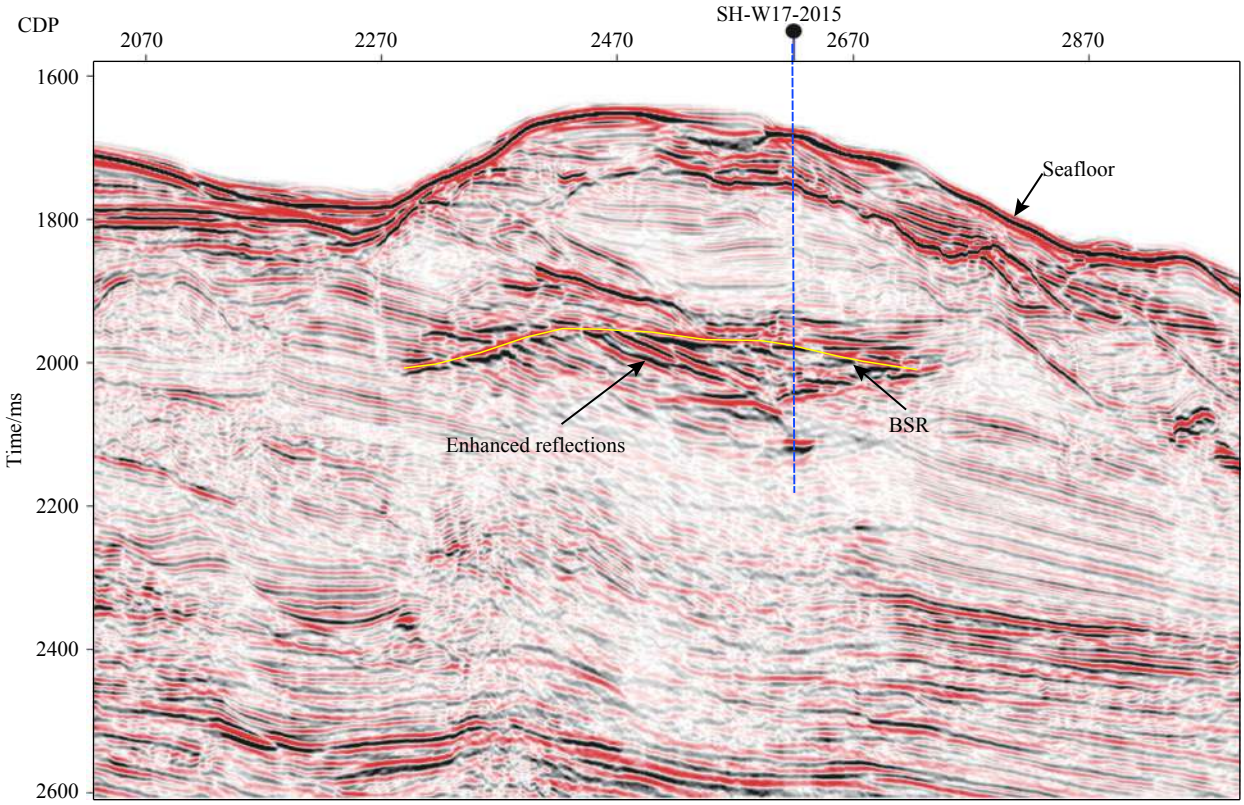

Fig. 3. The BSR features in the seismic profile across the station SH-W17-2015.

amplitude energy, strong continuity and negative polarity (Fig. 4a, 4b). The AVA characteristics of BSR extracted from common image gathering show that the relative amplitude decreases with the increase of the incident angle, which is the AVA characteristic of type IV (Fig. 4c). This indicates that the contribution of NGH to BSR is relatively large. According to the results of pore water desalination near the drilling site (SH-W18-2015), the maximum saturation of NGH is 63%, and the average value is above 40%. The saturation of free gas in the underlying formation of BSR interpreted by logging is about 7%.

The presence of BSR is generally interpreted as NGH. Still, current studies have shown that there is no direct relationship between NGH and BSR (Yang R et al., 2013), in other words, the presence of NGH has also been found in areas without BSR (for example, the Gulf of Mexico). Seismic attenuation is another method for identifying hydrate and free gas. NGH and free gas sediments with a certain thickness and saturation will cause strong attenuation of high frequency components of seismic data (Guerin G and Goldberg D, 2013; Zhang RW et al., 2016; Nittala S et al., 2017; Kumar J et al., 2018). By choosing the appropriate frequency spectrum decomposition algorithm, seismic data are divided into frequency processing, and the reflection energy of the formation near BSR is observed in different frequency domains. It can accurately detect the high frequency attenuation characteristics of hydrate and free gas sediment, so as to find the favorable development areas of hydrate and free gas. Fig. 5 is a high-frequency seismic attenuation profile of station SH-W11-2015. Obvious attenuation characteristics are shown in the up and down of the BSR. The thickness of gas hydrate layer corresponds well with the high-frequency attenuation.

4. Gas hydrate inversion

4.1. Logging data analysis

Before seismic inversion, it is necessary to normalize and analyze logging-while-drilling (LWD) data in the production test area to confirm whether the NGH reservoir section has obvious wave impedance anomalies. Fig. 6 shows the well logging curve of station SH-W11-2015 and the distribution of NGH saturation. The saturation value comes from the chloride ion desalination analysis data of pore water. NGH occur roughly between 1426–1507 m in distribution. The thickness of gas hydrates is about 81 m. The average gas hydrate saturation is about 34% and the maximum gas hydrate saturation is 53%. In the region of NGH distribution, the characteristics of the resistivity curve increase, acoustic and shear wave slowness are obvious.

Combined with the analysis results of the LWD data, the acoustic wave impedance of the GH reservoir is obviously different from that of the non-gas hydrate reservoir. According to the wave impedance histogram, when the wave impedance value is greater than 2970 m/s·g/cm^3, the NGH reservoir is dominant (Fig. 7). It shows that the wave impedance can effectively distinguish the NGH reservoir from the non-hydrate reservoir. It also shows that the wave

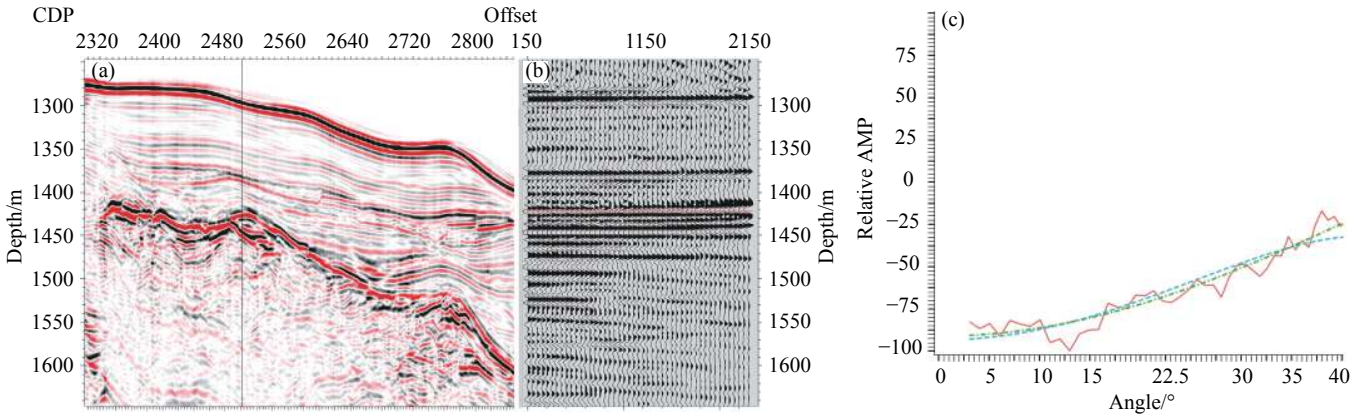

Fig. 4. Seismic migration stack section (a), common imaging gathering (b) and AVA characteristics of BSR (c) of Inline 96 (red solid line: actual amplitude change curve; blue dotted line: Shuey formula fitting curve; green dotted line: Aki & Richards formula fitting curve).

impedance inversion is credible to predict the distribution of NGH.

4.2. Method and results

Different methods can be used for the wave impedance inversion of post-stack seismic data, such as band-limited inversion, sparse spike inversion and model-based inversion, etc. (Riedel M and Shankar M, 2012). Band-limited impedance inversion uses the classical recursive inversion algorithm, but ignores the influence of seismic wavelet, simply regards seismic trace as a group of reflection coefficients and adds low-frequency components from logging curves. The sparse spike inversion method takes the reflectivity as a minimum series of spikes until the matching accuracy of the seismic trace is sufficient, but its result is too simple to model. Although it can well meet the seismic data, the result is usually a single geological law. The model-based inversion uses a generalized linear inversion algorithm, which tries to modify the initial model until the synthetic record matches the seismic trace within an acceptable range (Russell B and Hampson D, 1991). This method has certain knowledge of geological conditions and can establish reliable models.

In this paper, the model-based inversion method is used. The initial model is derived from four LWD data (SH-W18-2015, SH-W19-2015, SH-W11-2015 and SH-W17-2015) and accurate horizon interpretation information. The model-based inversion needs to calibrate the target horizons with the initial Ricker wavelet firstly. On the basis of the well-seismic calibration, the seismic wavelet is extracted from the seismic data and well curves, and the synthetic seismic records are reproduced with the wavelet, and the time-depth relationship is constantly revised so that the synthetic seismic records and the bypass seismic data can be reached.

According to the wave impedance inversion results of the station SH-W17-2015 and SH-W11-2015 (Fig. 8 and Fig. 9), the vertical distribution of NGH coincides with the actual

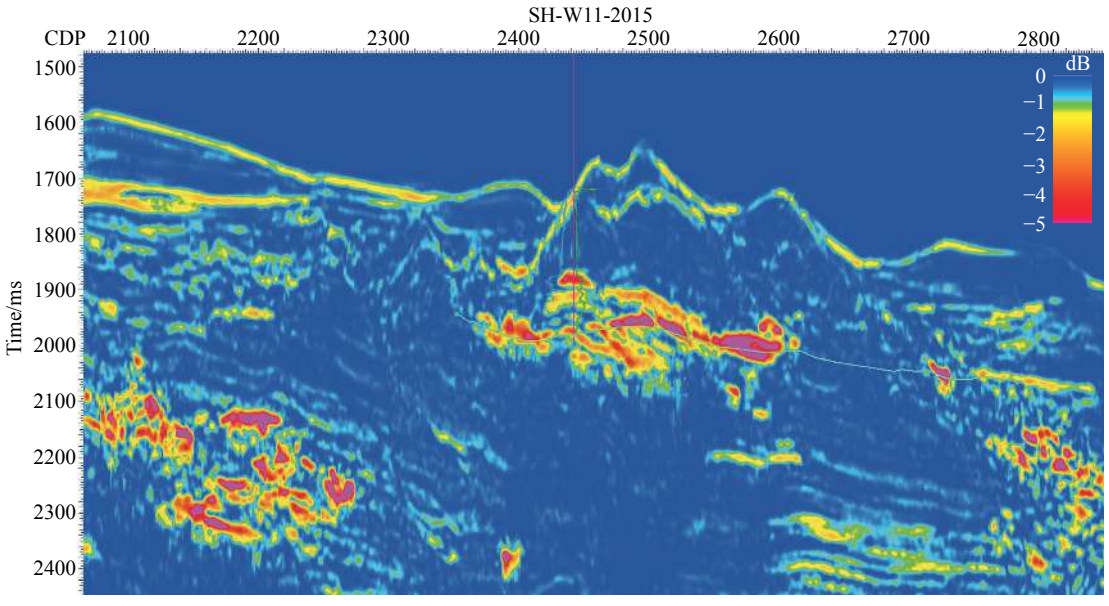

Fig. 5. Seismic high-frequency attenuation attribute profile of station SH-W11-2015.

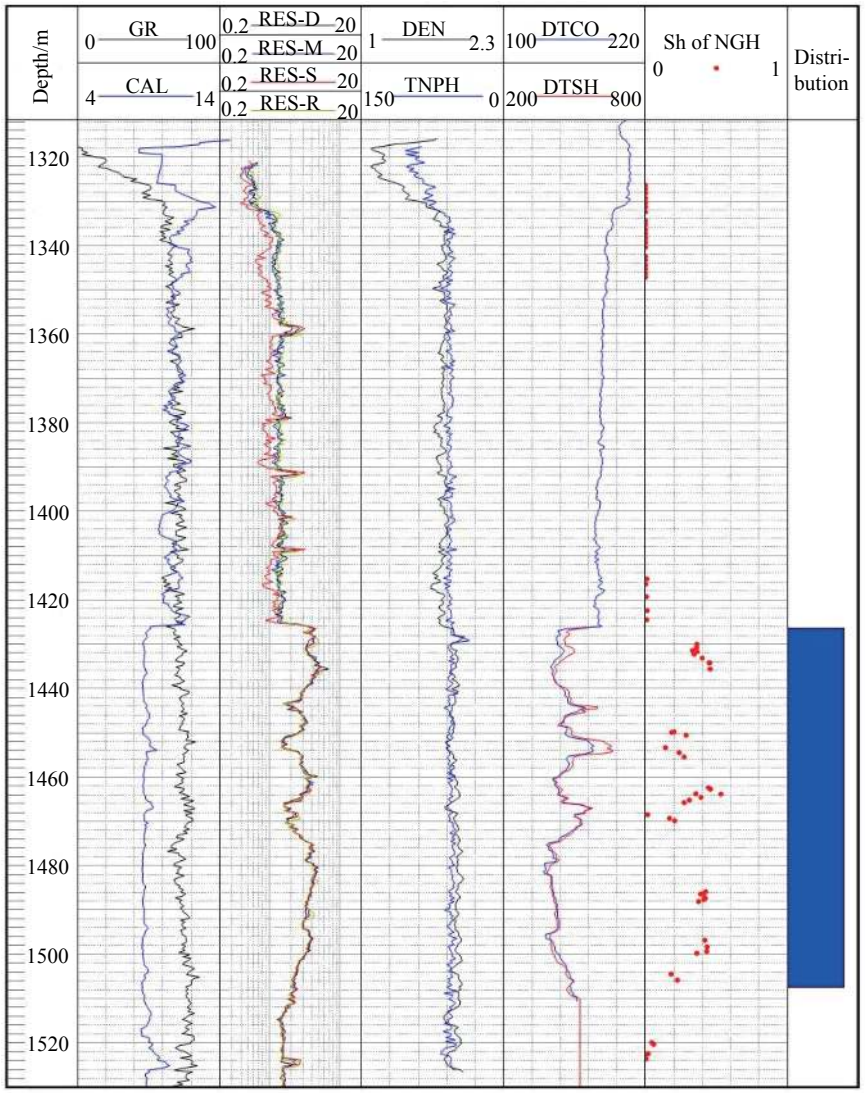

Fig. 6. Logging curve and the hydrate saturation distribution of station SH-W11-2015.

drilling. The NGH reservoir thicknesses of SH-W17-2015 and SH-W11-2015 wells are 30 m and 81 m respectively. NGH reservoirs are distributed continuously in the form of a flying saucer, which is a favorable distribution area of NGH.

5. Gas hydrate reservoir distribution

According to the impedance inversion results of model-based inversion, the top and bottom interfaces of NGH reservoirs are traced and characterized carefully, and the planar distribution maps of the two NGH reservoirs in Fig. 10 are obtained. There are mainly two NGH orebodies in the Shenhu production test area, one of which is mainly controlled by the drilling sites SH-W18-2015 and SH-W19-2015 (marked No.1 NGH orebody), the other is mainly controlled by drilling sites SH-W11-2015 and SH-W17-2015 (marked No.2 NGH orebody). All of them are characterized by a nearly north-south striped distribution and are characterized by an intermediate thickness and thin edges. The overall thickness of the No.1 NGH orebody is much lower than the No.2 orebody, but its distribution area is wider.

By calculating the distribution area and average effective thickness of the hydrate reservoir, the distribution area of the No.1 NGH orebody controlled by W18/W19 is about 11.24 km^2, the average effective thickness is 19 m, and the maximum thickness is 39 m; the distribution area of the No.2 NGH orebody controlled by W11/W17 is about 6.42 km^2, and the average effective thickness is 26 m, the maximum thickness is 90 m (Fig. 10).

In terms of the occurrence scale of NGH, the two orebodies are basically the same, but because NGH in the production test area is hosted in clayey silt, the permeability of the sediment is very poor, and the prediction of the influence of the production test on the decomposition of the scope will not be too large. Therefore, the thickness of the NGH orebody, rather than the distribution area, will be considered first. From this point of view, the No.2 NGH orebody will be better than the No.1 orebody.

6. Discussion

The drilling results of well Mallik 5L-38 in the Mackenzie

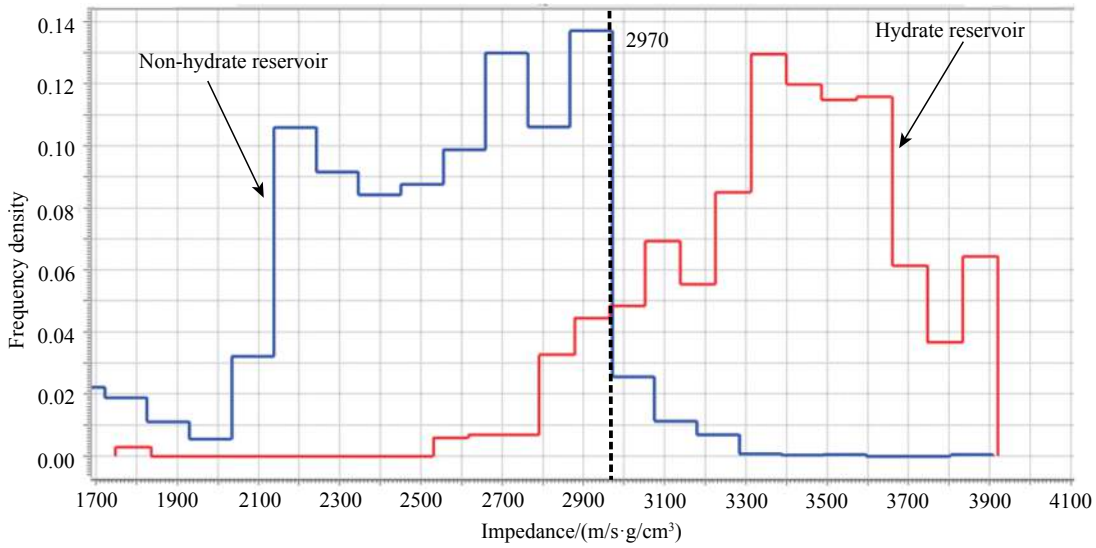

Fig. 7. Wave impedance histogram of hydrate bearing sediments and hydrate free sediments.

Delta of Canada (Collett TS et al., 2009; Dallimore SR and Collett TS, 2005; Zhang XH et al., 2014) show that the lithology of NGH reservoir is thickly-layered sandstone interbedded with conglomerate and siltstone layer. The saturation of NGH is from 50% to 90%, the porosity is about 40%, and the permeability is from 100 mD to 1000 mD.

The lithology of the drilled samples on the north slope of Alaska is mainly thick-layered sandstone. The porosity of the sediments is 40%, the absolute permeability is 1000 mD and the hydrate saturation is about 70% (Anderson B et al., 2014; Schoderbek D and Boswell R, 2011; Zhang XH et al., 2014).

According to the first NGH production test in the Nankai Trough of Japan, the lithology of the NGH reservoir is the interbedding of coarse sand and silt. The saturation of NGH is from 60% to 80%, the porosity is from 40% to 50%, and the permeability is from 47 mD to 840 mD (Fujii T et al., 2015).

Well logs from the Green Canyon 955 H (GC955-H) in the northern Gulf of Mexico (GOM) well indicate that there are two types of gas hydrate reservoirs encountered in this well. One type is the fracture-filling gas hydrate in clay-bearing sediments with anisotropic physical properties (the average gas hydrate saturations of about 20%) and the other is pore-filling gas hydrate in sands with assumed isotropic physical properties (the saturation reaches about 70%) (Lee MW and Collet TS, 2012).

NGH was discovered in the Krishna-Godavari (KG) Basin during the India National Gas Hydrate Program (NGHP) Expedition 1 at Site NGHP-01-10 within a fractured clay-dominated sedimentary system. NGH saturations are greater than 50% (as high as 80%) of the pore space for the depth interval between 25–160 m below the seafloor (Lee MW and Collet TS, 2009, Riedel M et al., 2010).

Boswell R (2009) proposed a "Gas Hydrates Resource Pyramid " model, described qualitatively the positive

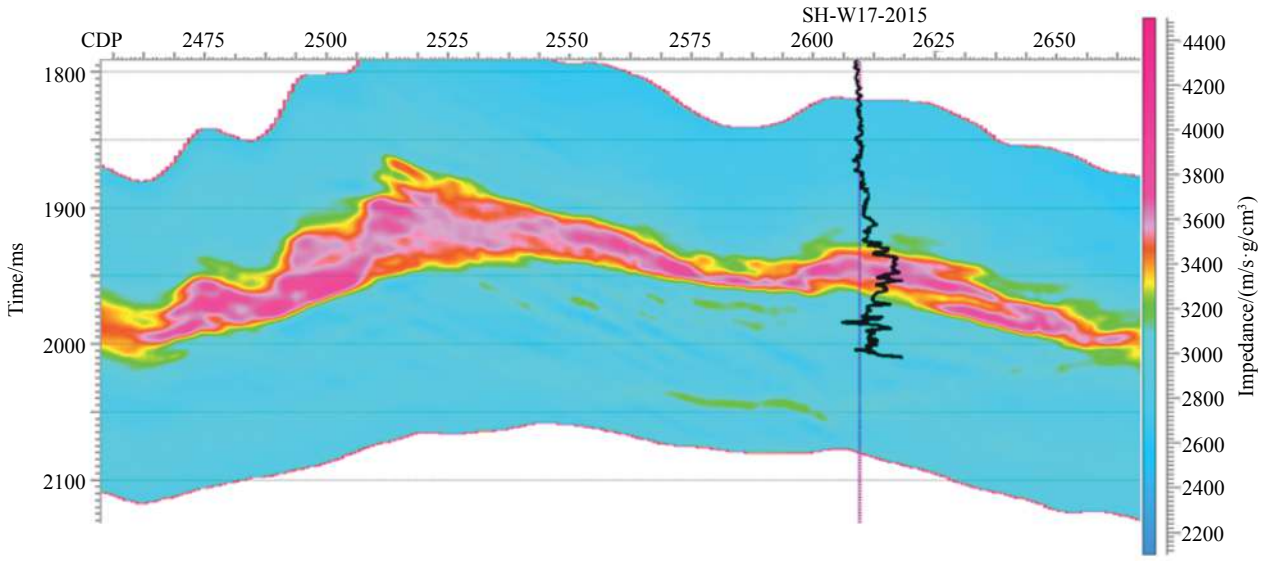

Fig. 8. Impedance inversion profile of inline in the station SH-W17-2015.

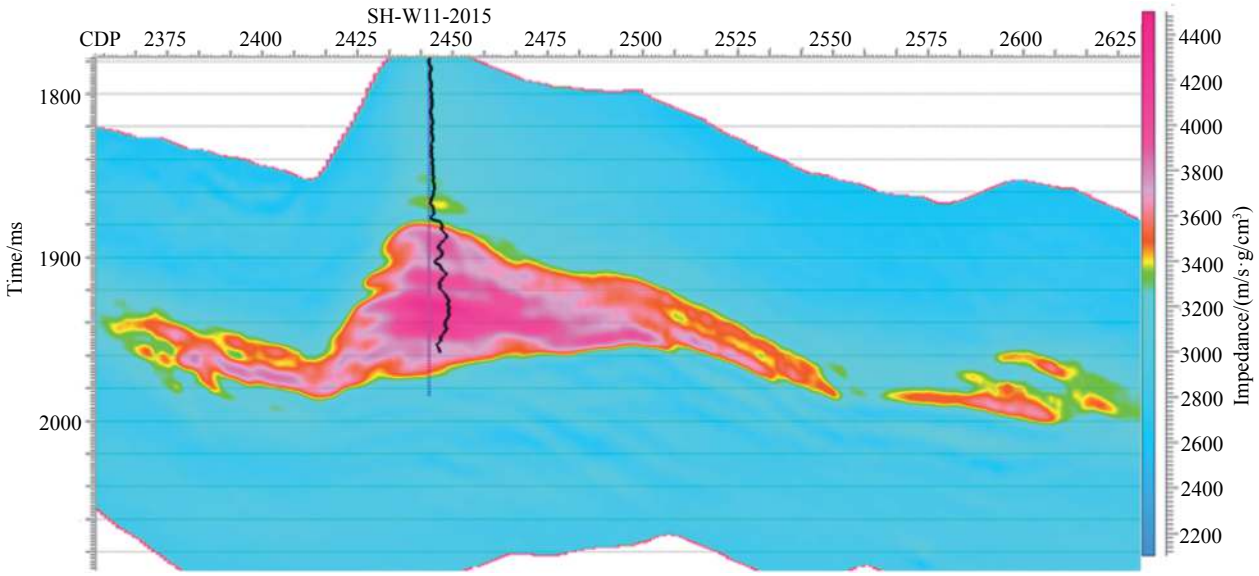

Fig. 9. Impedance inversion profile of inline in the station SH-W11-2015.

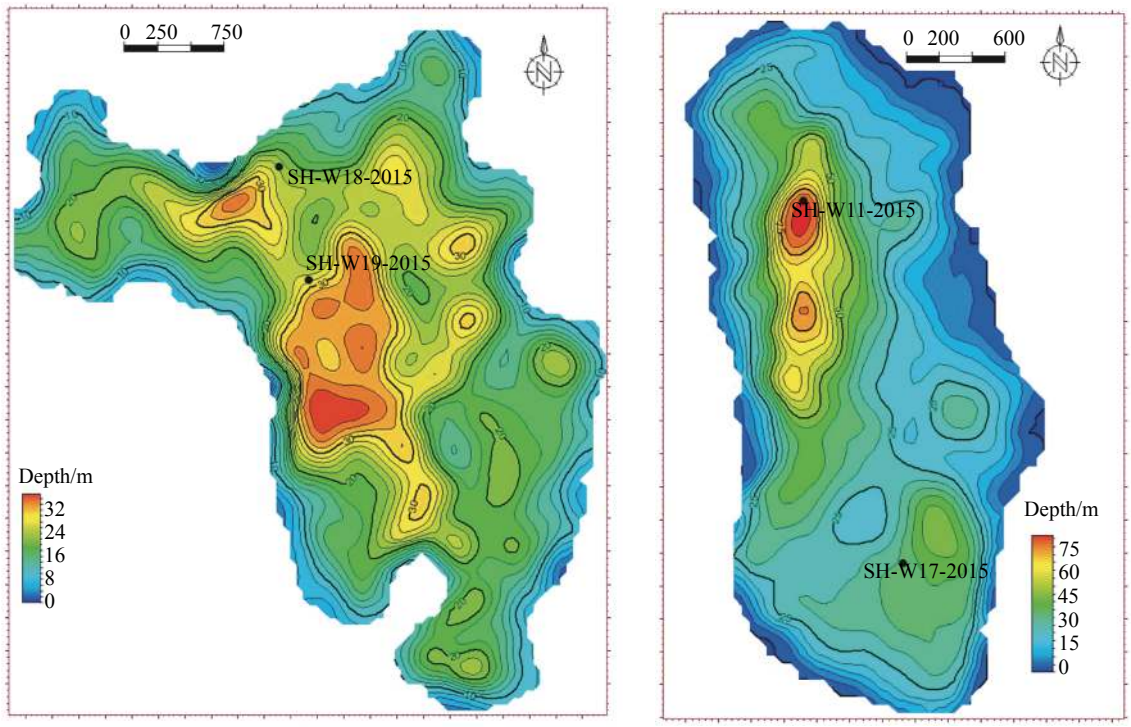

Fig. 10. The thickness distribution map of two gas hydrate deposits in the production test area of the Shenhu area.

correlation between various types of NGH reservoir resource potential and the difficulty of exploitation, pointed out the direction for the production of NGH. From the top to the bottom of this pyramid, the resource potential of all kinds of reservoirs increases gradually, but the resource grade decreases gradually, the reliability of resource prediction decreases correspondingly, the difficulty of exploitation increases correspondingly, and the recoverable efficiency decreases gradually (Wu NY et al., 2017). For the pyramid, it is difficult to exploit NGH from low to high, which are conglomerate reservoirs (Canada, Alaska), sandy reservoirs (Japan, MOG), permeable clay reservoirs (containing structural, fracture-filled NGH) (India, MOG), cold seep-related massive reservoirs and non-permeable clay reservoirs (China). Because of the low saturation and permeability, the NGH reservoir in the Shenhu area of China, is very difficult for exploitation, which is very different from those production test areas in the USA, Canada and Japan (Li JF et al., 2018) (Fig. 11).

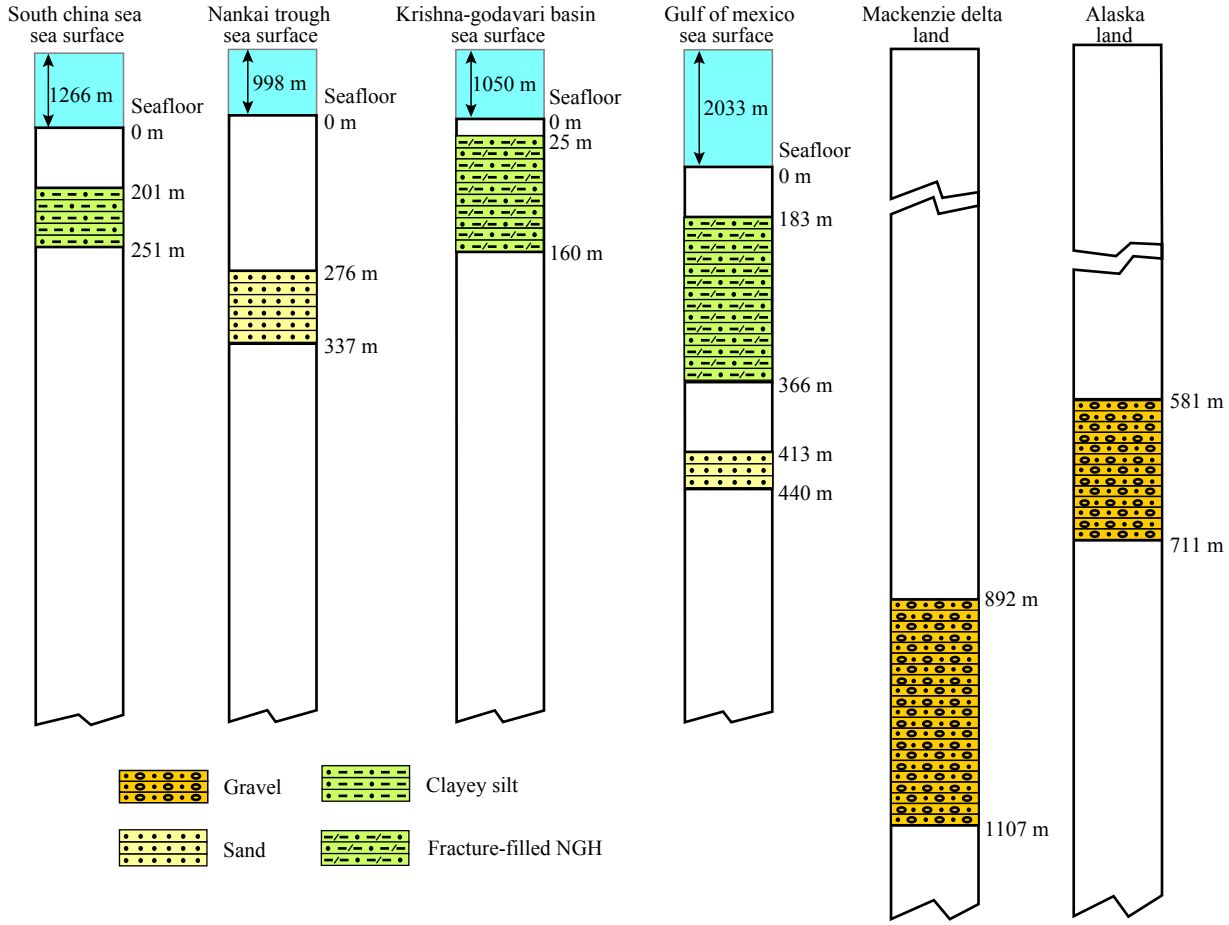

Fig. 11. The cartoon of reservoirs from global production test deposits (modified from Li JF et al., 2018).

7. Conclusions

According to research and comparison, the NGH reservoir in the Shenhu area, is mainly composed of fine-grained clay silt with low permeability, and very difficult for exploitation, which is very different from those discovered in the USA, Canada, India, MOG and Japan.

Wave impedance is the best attribute to distinguish NGH reservoirs from marine sediment. Based on the model-based seismic impedance inversion method, the initial impedance model is constructed by using the impedance data of LWD and the horizon interpreted by borehole seismic calibration, and the final impedance inversion result is achieved after several iterations.

There are mainly two NGH orebodies in the Shenhu production test area, which are distributed in a north-south direction and tend to be thicker in the middle and thinner at the edge. One orebody is thicker, but its area is narrower. Combined with the lithologic of the NGH reservoir, it has poor permeability. Therefore, the thickness of gas hydrate should be considered first in the production test, not the distribution area, when selecting the NGH orebody, and the hydrate orebody controlled by W11/W17 is better than that controlled by W18/W19.

Acknowledgment

The research was funded by the China National Project "Natural Gas Hydrate Exploration and Production Test" (DD20189310). The hydrate data processing research team (HDPRT) of GMGS reprocessed 3D seismic data, their work makes the imaging of seismic data clearer, the engineers He SY and Zhou ZZ gave their support and discussion on the geological interpretation work, and the anonymous reviewers, Dr. Yang Yan gave valuable suggestions and comments on the manuscript, which is greatly appreciated.

References

Anderson B, Boswell R, Collett TS, Farrell H, Ohtsuki S, White M, Zyrianova M. 2014. Review of the findings of the Ignik Sikumi CO2-CH4 gas hydrate exchange field trial. Proceedings of the 8th International Conference on Gas Hydrates (ICGH8–2014), Beijing, China.

Auguy C, Calvès G, Calderon Y, Brusset S. 2017. Seismic evidence of gas hydrates, multiple BSRs and fluid flow offshore Tumbes basin, Peru. Marine Geophysical Research, 38(4), 409–423. doi: 10.1007/s11001-017-9319-2.

Boswell R. 2009. Is gas hydrate energy within reach? Science, 325, 957–958. doi: 10.1126/science.1175074.

Carcione JM, Tinivella U. 2000. Bottom-simulating reflectors: seismic velocities and AVO effects. Geophysics, 65(1), 54–67. doi: 10.1190/1.1444725.

Chand S, Minshull TA, Gei D, Carcione JM. 2010. Elastic velocity models for gas‐hydrate‐bearing sediments - a comparison. Geophysical Journal of the Royal Astronomical Society, 159(2), 573–590.

Collett TS, Johnson AH, Knapp CC, Boswell R. 2009. Natural gas hydrates - Energy resource potential and associated geologic hazard. AAPG Memoir 89, 29(2), 858–869.

Dallimore SR, Collett TS. 2005. Scientific results from the Mallik. Scientific Results from the Mallik 2002 Gas Hydrate Production Research Well Program, Mackenzie Delta, Northwest Territories. Canada. Bulletin of the Geological Survey of Canada, 585(CD ROM), 957.

Dewangan P, Mandal R, Jaiswal P, Ramprasad T, Sriram G. 2014. Estimation of seismic attenuation of gas hydrate bearing sediments from multi-channel seismic data: A case study from Krishna-Godavari offshore basin. Marine & Petroleum Geology, 58, 356–367.

Ecker C, Dvorkin J, Nur A. 1998. Sediments with gas hydrate: Internal structure from seismic AVO. Geophysics, 63, 1659 –1669. doi: 10.1190/1.1444462.

Ecker C, Dvorkin J, Nur A. 2000. Estimating the amount of gas hydrate and free gas from marine seismic data. Geophysics, 65, 565 –573. doi: 10.1190/1.1444752.

Ehsan MI, Ahmed N, Din ZU, Khalid P, Wei LX. 2016. An application of AVO derived attributes to analyze seismic anomalies of gas hydrate bearing sediments in makran offshore, Pakistan. Acta Geodaetica Et Geophysica, 51(4), 1–13.

Fu SY, Lu JA. 2010. The characteristics and origin of gas hydrate in the Shenhu area, South China Sea. Marine Geology Letters, 26(9), 6–10 (in Chinese with English abstract).

Fujii T, Suzuki K, Takayama T, Tamaki M, Komatsu Y, Konno Y, Yoneda J, Yamamoto K, Nagao J. 2015. Geological setting and characterization of a methane hydrate reservoir distributed at the first offshore production test site on the Daini-Atsumi Knoll in the eastern Nankai Trough, Japan. Marine and Petroleum Geology, 66(2), 310–322.

Gei D, Carcione JM. 2003. Acoustic properties of sediments saturated with gas hydrate, free gas and water. Geophysical Prospecting, 51(2), 141–158. doi: 10.1046/j.1365-2478.2003.00359.x.

Gong YH, Yang SX, Wang HB, Liang JQ, Guo YQ, Wu SG, Liu GH. 2009. Gas hydrate reservoir characteristics of the Shenhu area, northern slope of the South China Sea. Geoscience, 23(2), 210–216 (in Chinese with English abstract).

Guerin G, Goldberg D. 2013. Modeling of acoustic wave dissipation in gas hydrate-bearing sediments. Geochemistry Geophysics Geosystems, 6(7), 542–557.

Guo YQ, Yang SX, Liang JQ, Lu JA, Lin L, Kuang ZG. 2017. Characteristics of high gas hydrate distribution in the Shenhu area on the northern slope of the South China Sea. Earth Science Frontiers, 24(4), 24–31.

Horozal S, Bahk JJ, Urgeles R, Kim GY, Cukur D, Kim SP, Lee GH, Lee SH, Ryu BJ, Kim JH. 2017. Mapping gas hydrate and fluid flow indicators and modeling gas hydrate stability zone (GHSZ) in the ulleung basin, east (Japan) sea: potential linkage between the occurrence of mass failures and gas hydrate dissociation. Marine & Petroleum Geology, 80, 171–191.

Jin JP, Wang XJ, Chen RX, Guo YQ, Su PB, Liang JQ, Qin J. 2017. Distribution of gas hydrate in the Shenhu area: identified with well log and seismic multi-attributes. Marine geology and Quaternary geology, 37(5), 120–130 (in Chinese with English abstract).

Jin QH, Zhang GX, Yang MZ. 2006. Introduction to gas hydrate resource. Science Press, China, 2 –36 (in Chinese with English abstract).

Katzman R, Holbrook WS, Paull C K. 1994. Combined vertical-incidence and wide-angle seismic study of a gas hydrate zone, Blake Ridge. J. Geophys. Res., 99, 17975–17995. doi: 10.1029/94JB00662.

Kuang ZG, Guo YQ. 2011. The sedimentary facies and gas hydrate accumulation models since Neogene of the Shenhu Sea area, Northern South China Sea. Earth Science-J. China University of Geosciences, 36(5), 915–920 (in Chinese with English abstract).

Kumar J, Sain K, Arun KP. 2018. Seismic attributes for characterizing gas hydrates: a study from the Mahanadi offshore, India. Marine Geophysical Research, 1, 1–14.

Lee MW, Collett TS. 2009. Gas hydrate saturations estimated from fractured reservoir at Site NGHP-01-10, Krishna-Godavari Basin, India. J. Geophys. Res., 114, 1–13.

Lee MW, Collett TS. 2012. Pore- and fracture-filling gas hydrate reservoirs in the Gulf of Mexico Gas Hydrate Joint Industry Project Leg II Green Canyon 955 H well. Marine and Petroleum Geology, 34, 62–71. doi: 10.1016/j.marpetgeo.2011.08.002.

Lei XM, Zhang GX, Zeng Y. 2009. Geological factors of the formation and distribution of natural gas hydrate in the north of Shenhu area, South China Sea. Marine Geology Letters, 25(5), 1–5.

Li JF, Ye JL, Qin XW, Qiu HJ, Wu NY, Lu HL, Xie WW, Lu JA, Peng F, Xu ZQ, Lu C, Kuang ZG, Wei JG, Liang QY, Lu HF, Kou BB. 2018. The first offshore natural gas hydrate production test in South China Sea. China Geology, 1, 5–16. doi: 10.31035/cg2018003.

Li W, Yu XH, Zeng XM, Wang JZ, Sang X. 2013. Study of Neocene seismic and sedimentary faces in the hydrate survey area of the Shenhu region on the north margin of South China Sea. Marine Geology Frontiers, 29(1), 17–26 (in Chinese with English abstract).

Liang J, Wang MJ, Lu JA, Liang JQ, Wang HB, Kuang ZG. 2013. Characteristics of sonic and seismic velocities of gas hydrate sediments in the Shenhu area, northern South China Sea. Natural Gas Industry, 33(7), 29–35 (in Chinese with English abstract).

Ma ZT, Gen JH, Dong LG, Song HB. 2002. Study on the seismic identification of marine gas hydrates. Marine Geology & Quaternary Geology, 22(1), 1–8 (in Chinese with English abstract).

Nittala S, Sain K., Nara D. 2017. Seismic vis-a-vis sonic attenuation in gas hydrate bearing sediments of Krishna Godavari basin, eastern margin of India. Geophysical Journal International, 209, 1195–1203. doi: 10.1093/gji/ggx089.

Riedel M, Collett TS, Kumar P, Sathe AV, Cook A. 2010. Seismic imaging of a fractured gas hydrate system in the Krishna-Godavari Basin offshore India. Marine and Petroleum Geology, 27, 1476–1493. doi: 10.1016/j.marpetgeo.2010.06.002.

Riedel M, Shankar M. 2012. Combining impedance inversion and seismic similarity for robust gas hydrate concentration assessments - A case study from the Krishna-Godavari basin. Marine and Petroleum Geology, 36, 35 –49. doi: 10.1016/j.marpetgeo.2012.06.006.

Russell B, Hampson D. 1991. Comparison of poststack inversion methods. 61st Annual International Meeting, SEG, Expanded Abstracts, 10, 876–878.

Schoderbek D, Boswell R. 2011. IgnIk Sikumi #1, Gas hydrate test well, successfully installed on the Alaska North slope. Fire in the Ice, Methane Hydrate Newsletter, 11(1), 1–5.

Sha ZB Liang JQ, Su PB, Zhang GX, Lu JA, Wang JL. 2015. Natural gas hydrate accumulation elements and drilling results analysis in the eastern part of the Pearl River Mouth Basin. Earth Science Frontiers, 22(6), 125–135 (in Chinese with English abstract).

Singh SC, Minshull TA, Spence GD. 1993. Velocity structure of a gas hydrate reflector. Science, 260(5105), 204–207. doi: 10.1126/science.260.5105.204.

Sloan ED. 1990. Clathrate Hydrates of Natural Gases. New York: Marcel Dekker, Inc.

Song HB, Hao TY, Song LX, Wu NY. 2001. Geophysical researches on marine gas hydrates (I): physical properties. Progress in geophysics, 16(2), 118–126 (in Chinese with English abstract).

Song HB, Zhang L, Jiang WW, Hao TY. 2003. Geophysical researches on marine gas hydrates(Ⅲ): bottom simulating reflections. Progress in geophysics, 18(2), 182–187 (in Chinese with English abstract).

Su PB, Liang JQ, Sha ZB, Fu SY. 2014. Gas sources condition of gas hydrate formation in the Shenhu deep water sea zone. Journal of Southwest Petroleum University: Science & Technology Edition, 36(2), 1–8 (in Chinese with English abstract).

Su PB, Liang JQ, Zhang ZJ, Sha ZB. 2017. Analysis on the bright spots and dim out of seismic section for diffusion-type hydrate in the Shenhu area. Earth Science Frontiers, 4, 51 –56 (in Chinese with English abstract).

Wang JL, Liang JQ, Zong X, Gong YH, Wan TH. 2015. Differentiated distribution of methane hydrate in the Shenhu area of the northern South China Sea and controlling factors. Marine Geology Frontiers, 31(1), 24–30 (in Chinese with English abstract).

Wang LF, Lu JA, Liang JQ Shang JJ, Wang JL. 2017. Research on fluid migration rates derived from BSR at the hydrate drilling area off the northeastern slope of the South China Sea. Earth Science Frontiers, 24(4), 78–88 (in Chinese with English abstract).

Wu NY, Huang L, Hu GW, Li YL, Chen Q, Liu CL. 2017. Geological controlling factors and scientific challenges for offshore gas hydrate exploitation. Marine geology and Quaternary geology, 37(5), 1 –11 (in Chinese with English abstract).

Xu HN, Zhang GX, Zheng XD, Wang MJ, Yang SX, Yang R, Liang BW. 2014. Integrated analysis of well logs and seismic data to deduce the possible distribution in depth of gas hydrate in the Shenhu Area, South China Sea. Chinese Journal of Geophysics, 57(10), 3363–3372 (in Chinese with English abstract).

Yang R, Wu NY, B J, Su Z, Liang JQ, Sha ZB. 2013. Gas hydrate identification in non-BSR region, northern South China Sea. Progress in Geophysics, 28(2), 1033–1040 (in Chinese with English abstract).

Ye JL, Qin XW, Qiu HJ, Liang QY, Dong YF, Wei JG, Lu HL, Lu JA, Shi YH, Zhong C, Xia Z. 2018. Preliminary results of environmental monitoring of the natural gas hydrate production test in the South China Sea. China Geology, 1, 202–209. doi: 10.31035/cg2018029.

Yuan T, Nahar KS, Chand R, Hyndman RD, Spence GD, Chapman NR. 1998. Marine gas hydrates: Seismic observations of bottom-simulating reflectors off the west coast of Canada and the east coast of India. Geohorizons, 3(1), 235–239.

Zeng XM, Yu XH, Wang JZ, Kuang ZG. 2013. Controlling factors of natural gas hydrate in the north of the Shenhu area, South China Sea. Marine Geology Frontiers, 29(10), 31 –40 (in Chinese with English abstract).

Zhang GX, Liang JQ, Lu JA, Yang SX, Zhang M, Xu HN, Fu SY, Kuang ZG. 2014. Characteristics of natural gas hydrate reservoirs on the northeastern slope of the South China Sea. Natural Gas Industry, 34(11), 1–10 (in Chinese with English abstract).

Zhang GX, Xu HN, Liu XW, Zhang M, Wu ZL, Liang JQ, Wang HB, Sha ZB. 2014. The acoustic velocity characteristics of sediment with gas hydrate revealed by integrated exploration of 3D seismic and OBS data in the Shenhu area. Chinese Journal of Geophysics, 57(4), 1169–1176 (in Chinese with English abstract).

Zhang HT, Zhang HQ, Zhu YH. 2007. Research status and progress of gas hydrate in China. Geology in China, 34(6), 953–961 (in Chinese with English abstract).

Zhang RW, Zhang BJ, Huang HD, Xu HN. 2011. AVA characteristics of gas hydrate bearing sediments. Oil Geophysical Prospecting, 46(4), 634–639 (in Chinese with English abstract).

Zhang RW, Zhang BJ, Wei PF, Huang HD. 2012. Seismic correlation constrained multi-channel velocity inversion. Progress in Geophysics, 27(1), 326–334 (in Chinese with English abstract).

Zhang RW, Li HQ, Zhang BJ, Huang HD, Wen PF. 2015. Detection of gas hydrate sediments using prestack seismic AVA inversion. Applied Geophysics, 12(3), 453 –464. doi: 10.1007/s11770-015-0503-3.

Zhang RW, Li HQ, Wen PF, Zhang BJ. 2016. The velocity dispersion and attenuation of marine hydrate-bearing sediments. Chinese Journal of Geophysics, 59(9), 3417–3427 (in Chinese with English abstract).

Zhang RW, Zhang BJ, Huang HD, Wen PF. 2016. The method of marine residual multiple attenuation. Computing Techniques for Geophysical and Geochemical Exploration, 38(5), 666 –671 (in Chinese with English abstract).

Zhang W, Liang JQ, Lu JA, Wei JG, Su PB, Fang YX, Guo YQ, Yang SX, Zhang GX. 2017. Accumulation features and mechanisms of high saturation natural gas hydrate in the Shenhu Area, northern South China Sea. Petroleum Exploration and Development, 44(5), 670–680 (in Chinese with English abstract).

Zhang W, Liang JQ, Su PB, Wei JG, Sha ZB, Lin L, Liang J, Huang W. 2018. Migrating pathways of hydrocarbons and their controlling effects associated with high saturation gas hydrate in the Shenhu area, northern South China Sea. Geology in China, 45(1), 1 –14 (in Chinese with English abstract).

Zhang XH, Lu XB, Liu LL. 2014. Advances in natural gas hydrate recovery methods. Progress in Geophysics, 29(2), 858 –869 (in Chinese with English abstract).